JOM 23373

Formation of a high surface area, regular porous solid from the cluster of clusters, $Zn_4^{II}O[(CO)_9Co_3CCO_2]_6$

Wei Cen, Barbara Ladna, Thomas P. Fehlner

Department of Chemistry and Biochemistry, University of Notre Dame, Notre Dame IN 46556 (USA)

Albert E. Miller and Duofeng Yue

Department of Electrical Engineering, University of Notre Dame, Notre Dame IN 46556 (USA)

(Received June 18, 1992)

Abstract

The discrete molecular cluster of clusters, $Zn_4^{II}O[(CO)_9Co_3CCO_2]_6$ (1), undergoes thermolysis with the sequential loss of 54 CO and 6 CO_2 molecules without fusion resulting in the formation of a porous solid product. Density (fluid displacement and single crystal dimensions) and BET surface area measurements confirm the porous nature of the material. The calculated pore dimensions and regularity is corroborated by TEM of thermolyzed films supported on carbon. The formation of an α-Co phase is detectable by XRD and electron diffraction with crystallite size increasing with increasing heating temperature. The metallic nature of the cobalt environment is demonstrated by XPS of the films. Densification of the material occurs above 300°C with significant loss of surface area.

1. Introduction

In the use of molecular precursors [1–3] for ceramics, thin films and other materials, one would like to go beyond simple stoichiometry and attain control of some of the structural aspects of the solid materials. That is, complex single precursors can result in material properties that may not be accessible via a set of simpler precursors. Recent examples include the solid state pyrolysis of a molecular precursor leading to a kinetically stabilized form of AlN [4] and the vapor phase deposition of a molecular precursor leading to a new GaS phase [5]. In our own work utilizing metallaboranes as volatile CVD precursors to metal borides [6–9] stoichiometric control has been achieved and a preferred magnetic domain structure was described. In the following we present evidence that suggests that the internal framework of a non-volatile cluster of clusters is of consequence in determining the microstructure of the solid product formed during thermolysis.

Correspondence to: Dr. T.P. Fehlner.

We have already communicated the preparation and some of the properties of $Zn_4O[(CO)_9Co_3CCO_2]_6$ (1), (Fig. 1) [10]. This molecular solid can be prepared on a gram scale, is modestly soluble in THF, and forms single crystals containing one molecule of solvate per complex. Depending on crystallization conditions, crystals with sizes up to 2 mm can be obtained. As 1 contains CO and CO_2 moieties that should be readily lost as gaseous species on thermolysis, we have now examined the solid product in order to look for evidence of microstructure attributable to the precursor structure.

2. Experimental details

2.1. General

Reactions and manipulations were conducted under N_2 using standard Schlenk techniques. Glassware was oven-dried before use. Solvents were distilled from drying agents under nitrogen as follows: sodium benzophenone ketyl for hexane, diethyl ether and tetrahydrofuran (THF), $Co_2(CO)_8$ was from Strem and used directly. $Zn_4O[(CO)_9Co_3CCO_2]_6$ (1) was prepared as

0022-328X/93/$6.00

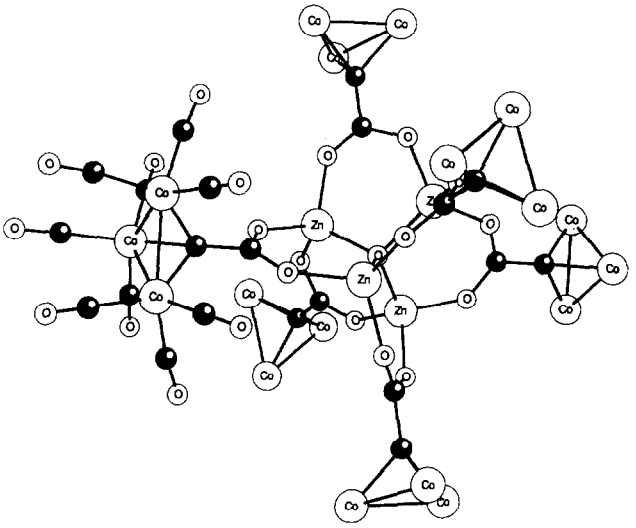

Fig. 1. Representation of the $Zn_4O[(CO)_9Co_3CCO_2]_6$ molecule (1). Note that the carbonyl ligands have been removed from five of the six cobalt clusters for clarity.

reported previously [10]. Elemental analyses were performed by Galbraith Laboratories, Knoxville, TN.

The experimental setup shown in Fig. 2 was used to simultaneously prepare samples of $Zn_4O[(CO)_9Co_3CCO_2]_6$ for the measurement of weight loss, displacement density, change in external particle dimensions, IR absorption and X-ray diffraction as a function of heating time and temperature. Under vacuum (10^{-6} torr), the temperature of all samples was increased slowly and maintained at the desired temperature for 12 h. After cooling to room temperature and back filling with Ar, sample tube A was weighed. This process was repeated until a constant weight of the sample in tube A was achieved. At this point the appropriate measurements were carried out on the other samples.

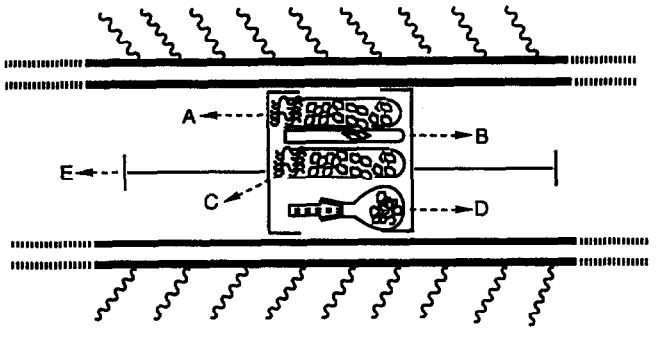

Fig. 2. Experimental setup for the equilibrium pyrolysis experiment. Shown is the middle section of a 3 cm diameter glass tube under dynamic vacuum in a tube oven. Tube for TGA experiment (A). Tube for change in external dimensions of large single crystals (B). Sample for IR measurements (C). Picnometer for displacement density measurements (D). Tube holders (E).

2.2. Equilibrium thermal gravimetric analysis

For the equilibrium thermogravimetric analysis, tube A was loaded with bulk crystalline **1** and plugged with glass wool in order to eliminate mechanical loss. For each step in temperature, the constant weight of tube A was recorded. Samples were heated in 12 h increments and most showed constant weight after two heating periods.

2.3. Density and dimension measurements

The buoyant density of crystals of **1** was measured with a mixture of CCl_4 and CBr_4. The displacement density (d_D) was measured with degassed hexane using a 1 cm^3 picnometer. After each density measurement, the residual hexane was removed under vacuum. Four big crystals with crystallographically characteristic shapes (1–2 mm) were chosen for the crystal dimension measurements. These crystals were put into tube B (5 mm in diameter) and heated along with the bulk sample A under the same conditions. After constant weight was achieved for the sample in tube A, the large crystals were taken out and the dimensional change was measured with an optical microscope. The apparent density (d_A) was calculated from the buoyant density (2.1 g cm^{-3}) of **1** and the averaged dimensional changes measured.

2.4. BET surface area measurements

The BET surface area for the sample crystals (average size of 0.5 mm) of $Zn_4O[(CO)_9Co_3CCO_2]_6$ was measured by single point BET (N_2) adsorption method with an automatic Quanta Chrome Monosorb instrument. A starting sample of about 1 g was used in order to achieve accurate measurement. The sample was loaded into a U tube and purged with N_2 for 0.5 h before measurement. Liquid N_2 was used for the cooling bath.

2.5. X-ray and IR measurements

The X-ray powder patterns were measured with a Philips X-ray powder diffraction system APD 3520; $30° \leq 2\Theta \leq 90°$, $\lambda = 1.5407$ Å. Infra-red spectral data were obtained on a Nicolet 205 FT-IR in KBr pellets.

2.5.1. 150–180°C

X-ray powder patterns: a very broad strong peak centered at ($2\theta = 46°$, d = 1.973 Å) with half width of 14°.

IR spectra: (KBr, 4000–400 cm^{-1}): OH: 3400m(br); COO^-: 1480vs, 1383vs; others: 1064w, 827w, 493m(br).

2.5.2. 300–330°C

X-ray powder patterns: d (Å) = 2.16, 2.04, 1.91, 1.49, 1.25 with average half width of 2° assigned to an α Co

phase with a calculated crystallite size of 90 Å according to the Scherrer formula.

IR spectra: (KBr, 4000–400 cm^{-1}): OH: 3400vw, br; COO^-: 1480w, 1383w; others: 1049vw, 1030vw, 830vw, 482w(br).

2.5.3. 400–440°C

X-ray powder patterns: d (Å) = 2.160, 2.042, 1.911, 1.492, 1.253 with average half width of 0.48° assigned to an α Co phase with a calculated crystallite size of 670 Å. In addition several weak lines were observed that could not be assigned. IR spectra: (KBr, 4000–400 cm^{-1}): 450s(br).

2.6. TEM measurements

The transmission electron microscopy (TEM) analysis was conducted on a Jeol 100CX instrument with an accelerating voltage of 120 KeV. The sample for this purpose was made by casting the material from a saturated THF solution on a copper grid covered with a carbon film. To examine the crystallization behavior of the material, the bright field images with corresponding diffraction patterns were taken for the different heat treatment conditions. The phase identification and the grain and pore size estimation were carried out on the TEM results.

2.7. XPS measurements

The X-ray photoelectron spectra (XPS) were measured in a Kratos XSAM 800 system. Mg Kα radiation at 1253.6 eV was used for the electron excitation and the spectra were collected with a hemispherical analyser. The sample was prepared in the form of a film cast from a saturated THF solution directly on a copper block. The copper block was then attached to the heater on the direct insertion probe. The temperature of the sample was measured with a calibrated thermocouple. Besides survey scans, the XPS of the Co(2p and 3p), Zn(2p and 3p), O(1s) and C(1s) ionization regions were collected at room temperature, after heating the sample at 200°C for 30 min, and after heating the sample at 200°C for 90 min. There were no qualitative differences between the last two sets of data.

3. Results

3.1. Thermolysis of 1

Preliminary thermogravimetric data on the thermolysis of 1 in argon have been reported [10]. A single weight loss corresponding to the loss of 54 CO and 6 CO_2 which was complete at 220°C was observed and the identities of the volatile products were proved by *in situ* mass spectrometry. The material prepared in the 160 to 250°C range is pyrophoric in air evidencing a high reactivity. This reactivity created problems in the chemical analysis of the solid. After protecting the solid from air, the best analysis for Co, Zn and C was 60.63, 14.30, 2.19 (obs'd); 75.21, 18.54, 5.11% (calc'd for $Co_{18}Zn_4C_6O$). However, for three independent runs with varying exposure to air the Co/Zn ratio of the solid product produced at 300°C is 4.24 ± 0.01. Thus, based on both the TGA results and the solid analytical results, we formulate the composition of the solid as $Co_{18}Zn_4C_6O$.

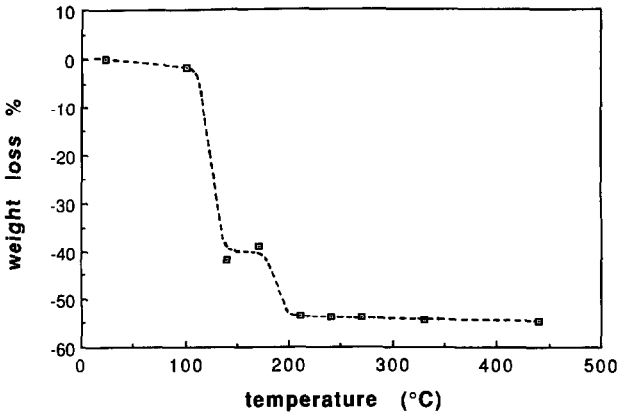

Fig. 3. Equilibrium thermal gravimetric analysis of $Zn_4O[(CO)_9Co_3CCO_2]_6$. Each point results from at least two heating periods and a minimum 12 h total equilibration time.

In order to eliminate kinetic factors in preparing the solid, the equilibrium (heating to constant weight at a given temperature under vacuum) thermogravimetric behavior was examined. A plot of the results (Fig. 3) shows a distinct plateau at $\approx 40\%$ weight loss and 160°C not observed in the normal TGA. The weight loss corresponds to ≈ 46 CO ligands. An additional weight loss corresponding to the remaining CO and 6 CO_2 molecules is observed at ≈ 180°C. IR measurements confirm this assignment. The IR of 1 exhibits both characteristic CO and carboxylate modes before thermolysis, wheras the product exhibits only the carboxylate modes when thermolysis is carried out at 160°C and neither CO nor carboxylate modes for thermolysis at 250°C. For pyrolysis carried out at 200°C and above the previously dark, dull appearance of the solid becomes metallic looking and the particles behave similarly to magnetized iron filings. Heating above 400°C under vacuum results in the formation of a metallic mirror deposit on the quartz tube. As this deposit dissolves in HCl with the formation of a gas, it results from the volatilization and deposition of Zn metal.

3.2. Density changes

Large individual single crystals of 1 retain their relative dimensions and characteristic geometric arrangement of faces and edges, but not X-ray diffrac-

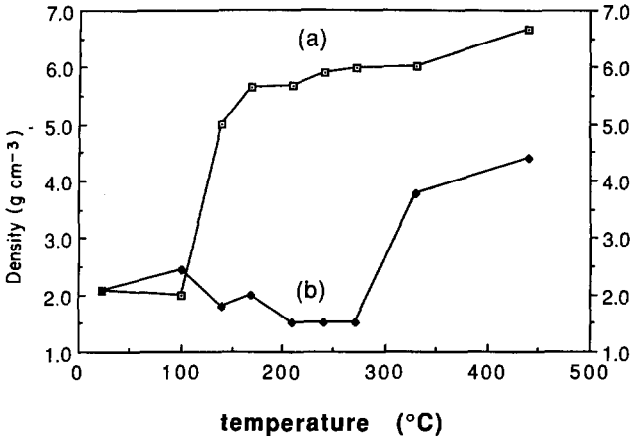

Fig. 4. Comparison of two measured densities (calculated as indicated in the text) of the product of the thermal decomposition of $Zn_4O[(CO)_9Co_3CCO_2]_6$ as a function of temperature. Curves (a) and (b) correspond to d_D and d_A, respectively.

tion properties, on thermolysis. Clearly the loss of ligands takes place without fusion. This phenomenon presented the opportunity of investigating the density change on thermolysis in two ways. A pair of equilibrium (as above) experiments were carried out simultaneously. First, the change in weight and dimensions (average edge shortening) of several large (1–2 mm) single crystals were used to calculate an apparent density (d_A) change as a function of thermolysis temperature. In the same experiment, the density of a 1 g polycrystalline sample with average crystal size of 0.5 mm was measured by hexane displacement (d_D). A comparison of the two densities is shown in Fig. 4. It is seen that although the displacement density change tracks the weight loss (major increase at $\approx$ 150°C), the relative density calculated from the crystal dimensions and weight shows much different behavior. By the latter measure, densification does not begin until $\approx$ 320°C. The implication is that the solid produced in the temperature range 150–320°C contains a considerable void volume. The void volume per gram can be calculated as $1/d_A - 1/d_D = 0.5$ cm^3/g. In the lower temperature regime the external crystal dimensions decrease about 15%. Major shrinkage of this porous structure with concurrent change in external dimensions of about 40% does not take place until 300°C where cobalt metal migration to form relatively large cobalt metal crystallites is observed (see below).

3.3. Surface area changes

In order to obtain more information on the nature of this internal volume, we have measured the surface area of the solid material by the BET method as a function of thermolysis temperature. The initial area of a 1.0 g sample of **1** with average particle size of 0.5 mm and after loss of the solvent of crystallization was 7.7 m^2/g. The surface area increased to an average value of 116 m^2/g between 160–220°C and then decreased to 50 m^2/g at 320°C when densification begins. Surface areas per unit weight for silica-gel range from 200–1000 m^2/g [11] and the surface area of "highly reactive" Ni powder has been reported as 33 m^2/g [12].

3.4. Pore size

The density and surface areas measurements allow one to estimate the average dimension of the pores. That is, the difference in surface areas before thermolysis (corrected for shrinkage) and at 160°C yields the internal surface area of the solid (110 m^2/g). Dividing the void volume per gram by this area yields the order of magnitude dimension of the pores of 45 Å. With the more specific assumption of long cylindrical channels one calculates an average radius of the pores of 90 Å. Above 300°C the volume based on particle size decreases as does the measured surface area leaving the calculated pore size approximately constant. This suggests that it is the number of pores that is decreasing on densification rather than their average size.

3.5. X-Ray diffraction

In order to gain more information on the changes in structure on heating **1** the X-ray diffraction (XRD) properties of the product were examined. The product formed at 150–180°C shows only very broad signals in the XRD whereas that formed after heating to 300–330°C and above shows the formation of small crystallites of α-Co estimated to be 90 Å in size from the FWHM of the diffraction lines. The same phase was observed at 400–440°C but with a calculated particle size of 670 Å.

3.6. Transmission electron microscopy

To obtain more spatial resolution in the diffraction properties of the material as well as direct information on particle and pore size, the solid product was examined by transmission electron microscopy (TEM). To do so a thin film of **1** was cast from a saturated THF solution on a metal grid supported carbon film. The film of **1**, which we take to represent a thin layer of the solid in the bulk material, was examined by TEM after several heat treatments. On thermolysis the film tends to curl and shrivel up creating tears and large holes. However, contiguous pieces of the pyrolyzed film, which were large on the TEM scale, could be examined. For a film treated at 150°C, Fig. 5 shows a diffuse electron diffraction pattern and basically a featureless TEM image. Heating to $\approx$ 230°C leads to a sharpening of the diffraction pattern and the TEM image at $\times$96,000 shows both grained particles and some large channels

corresponding to small tears in the film (Fig. 6). Higher magnification shows that the small channels are approximately 40 Å in width as are the particles themselves. The particle size distribution is narrow. Finally, in Fig. 7 heat treatment above 300°C leads to dotted rings in the diffraction pattern indicative of larger crystallites and the image shows larger particle size (100 Å) and a much broader particle size distribution. These observations are consistent with the initial formation of an essentially amorphous material with no observable microstructure by TEM; followed by rearrangement, presumably by diffusion, to yield a microporous material with fairly regular particle size and tiny cobalt crystallites; followed by further diffusion to yield much larger cobalt crystallites and less regular particle sizes.

3.7. X-Ray photoelectron spectroscopy

To probe the chemical environment of the metal atoms as a function of heat treatment we have examined films of **1** prepared similarly to those for TEM by X-ray photoelectron spectroscopy (XPS). However, in this case the films were formed on a heatable copper block and the pyrolysis of **1** was carried out in the reaction chamber of the XPS spectrometer. The extent of pyrolysis could be monitored by the C(1s) ionization associated with the CO and CO_2 moieties. As expected, after 30 min at 200°C the intensity of this ionization was reduced to zero. Unfortunately cracking

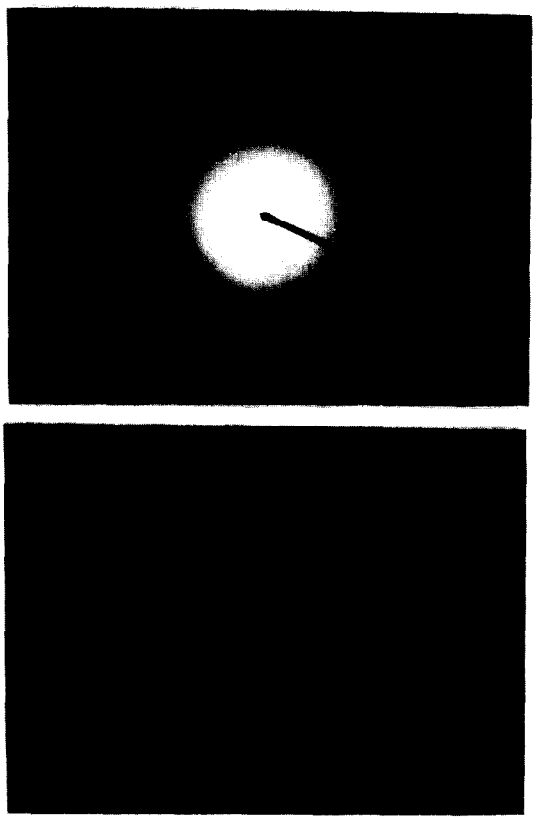

Fig. 5. (Top) The electron diffraction pattern for a $Zn_4O[(CO)_9Co_3CCO_2]_6$ film which was heated at 150°C for 2 h. (Bottom) Bright field image corresponding to the diffraction pattern and showing that no grained particles can be observed at ×96,000.

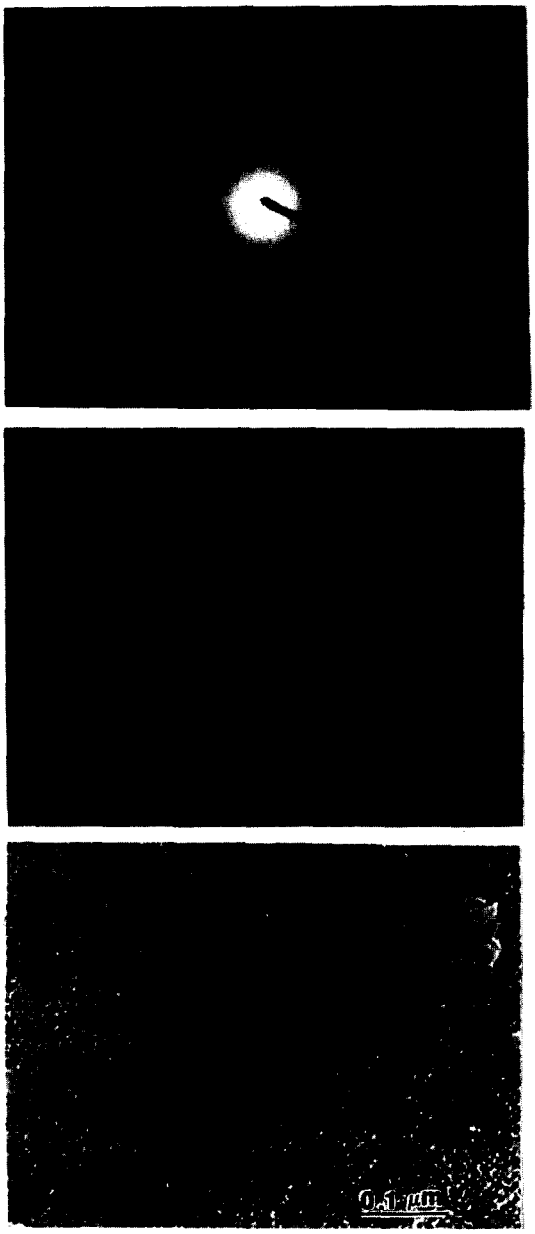

Fig. 6. (Top) The electron diffraction pattern for a $Zn_4O[(CO)_9Co_3CCO_2]_6$ film which was heated at 210–250°C for 4 h. Note the increase in the number of rings and their relative sharpness. (Middle) The bright field image (×96,000) corresponding to the diffraction pattern. The grained particles are uniformly formed and some large channels due to shrinkage tearing also can be observed. (Bottom) Enlarged area of the bright field image showing the small channels between the particles (≈ 40 Å) and the particles (≈ 40 Å).

of the film on pyrolysis exposed the copper block and did not allow quantitative determination of the carbon and oxygen remaining in the film. However, the Co(2p) and Zn(2p) ionizations were informative.

As shown in Fig. 8 both ionization energies shift to lower binding energy on heating but Co(2p) shifts 2.0 eV more. Indeed, when referenced to adventitious carbon, the binding energy of Zn(2p) increases by 0.1 eV whereas Co(2p) decreases by 1.9 eV. Referenced to carbon at 285.0 eV the Co(2p) and Zn(2p) energies are 780.0, 1121.5 and 778.1, 1121.6 eV in **1** and the heated sample, respectively. Using the CO carbon as a common internal reference, the Co(2p) binding energy for **1** is 0.5 eV lower than the literature gas phase value for $Co_2(CO)_8$ [13]. The Co(2p) binding energy for the metal is reported as 778.32 eV whereas that for the oxide is 780.4 eV [14]. Thus, the binding energy of the cobalt in the material produced from **1** is characteristic of a metallic environment. The binding energy of Zn metal is 1021.82 eV whereas that of ZnO is 1022.1 eV. Thus, the much lower sensitivity of the binding energy of Zn to environment does not allow any conclusions concerning the location and chemical environment of these atoms.

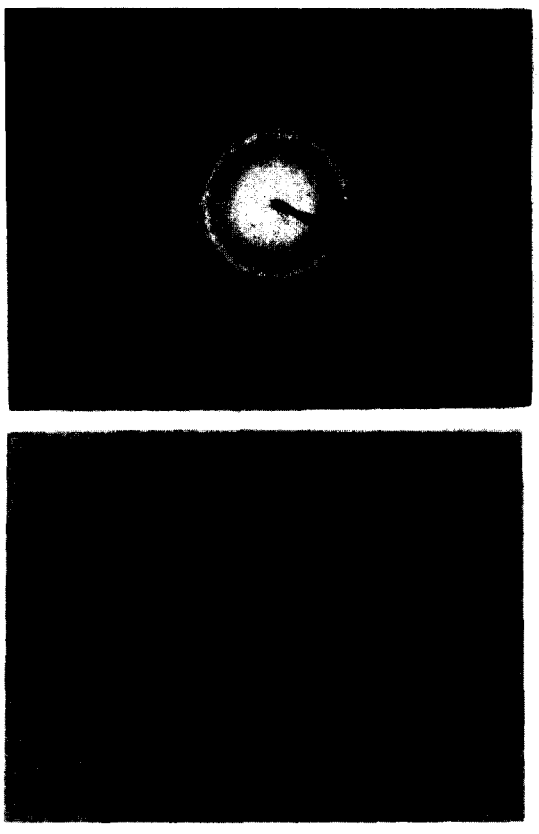

Fig. 7. (Top) The electron diffraction pattern for a $Zn_4O[(CO)_9Co_3CCO_2]_6$ film which was heated at 300–450°C for 4 h. The dotted rings show that the grains have grown in size. (Bottom) The bright field (×200,000) corresponding to the diffraction pattern shows an average particle size of ≈ 100 Å and a broader size distribution than that shown in Fig. 6.

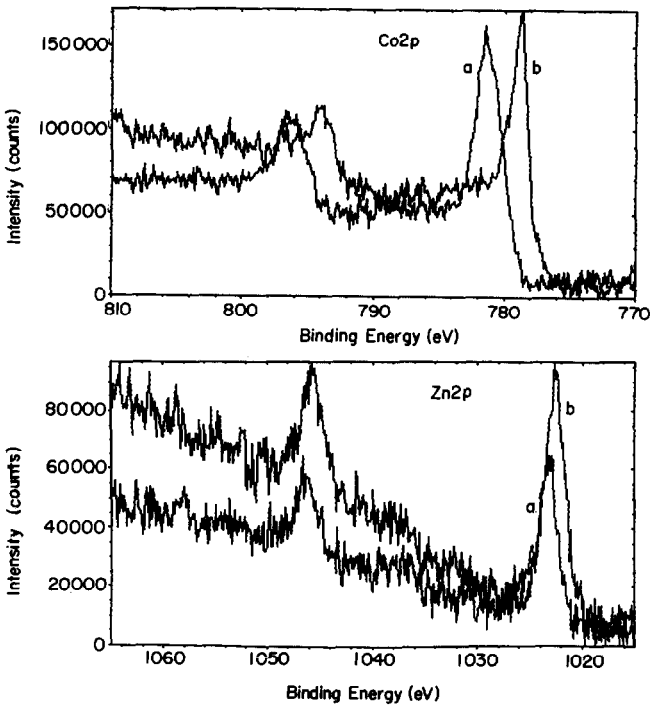

Fig. 8. (Top) The Co(2p) ionizations for **1** before heating (a) and after 30 min at 200°C (b). (Bottom) The Zn(2p) ionizations for **1** before heating (a) and after 30 min at 200°C (b).

4. Discussion

Based on the above experiments, we suggest that the formation and evolution of the material produced in the heating of **1** can be described as follows. First, the ≈ 24 Å in diameter spherical $Zn_4O[(CO)_9Co_3CCO_2]_6$ molecules, which are known to form a nearly close packed array in the solid state, shrink on loss of CO and CO_2 to form smaller cobalt-covered oxo-zinc-carboxylate cores with interparticle Co–Co bonds. This creates the large, measured void volume but the material first formed appears amorphous by TEM and XRD. However, the step in Fig. 2 and the IR results at 150°C show that the carboxylate moiety is still present which implies that the environment of the zinc atoms is similar to that in the molecular precursor. Continued heating at higher temperatures results in loss of the carboxylate ligands as CO_2 and in observable pore formation concurrent with the aggregation of the cobalt atoms into very small crystallites. The role of the zinc atoms is ambiguous but it is possible that they retain their association with the residual carbon and oxygen and support in some fashion the cobalt crystallites. Viewed in this sense, the network of regular pores

formed in the thermolysis of **1** is a remnant of the initial cluster of cluster structure that carries over into the product. Although cobalt crystallite growth continues, this porous microstructure is retained up to 300°C and suggests that the role of the Zn, C and O is an important one. Thus, one might view the material produced from heating **1** as a supported metal where both the support and the metal are derived from the single molecular precursor. High surface area supported metals are well known catalysts [15] and the material produced from **1** is presently being evaluated for such applications.

Acknowledgements

The support of National Science Foundation (TPF) is gratefully acknowledged as is partial support by the US Department of Energy, BES-Materials Sciences, under Contract W-32-109-Eng-38 at Argonne National Laboratory (AEM).

References

1 A. H. Cowley and R. A. Jones, *Angew. Chem., Int. Ed. Engl., 28* (1989) 1208.
2 H. D. Kaesz, R. S. Williams, R. F. Hicks, J. I. Znik, Y.-Y. Chen, H.-J. Müller, Z. Xue, D. Xu, D. K. Shuh and Y. K. Kuir, *New. J. Chem., 14* (1990) 527.
3 M. L. Steigerwald, T. Siegrist, S. M. Stuczynski and Y.-U. Kwon, *J. Am. Chem. Soc., 114* (1992) 3155.
4 W. L. Gladfelter, *Chemical Control of Nucleation and Growth in the Conversion of Molecules to Solid State Compounds*. 4th Chem. Congress of N. Amer., New York, 1991, pp. INORG 145.
5 A. N. MacInnes, M. B. Power and A. R. Barron, *Chem. Mater., 4* (1992) 11.
6 T. P. Fehlner, M. M. Amini, M. V. Zeller, W. F. Stickbe, O. A. Pringle, G. J. Long and F. P. Fehlner, *Mater. Res. Soc. Symp. Proc., 131* (1989) 413.
7 M. M. Amini, T. P. Fehlner, G. J. Long and M. Politowski, *Chem. Mater., 2* (1990) 432.
8 B. H. S. Thimmappa, T. P. Fehlner, G. J. Long and O. A. Pringle, *Chem. Mater., 3* (1991) 1148.
9 C.-S. Jun, T. P. Fehlner and G. J. Long, *Chem. Mater., 4* (1992) 440.
10 W. Cen, K. W. Haller and T. P. Fehlner, *Inorg. Chem., 30* (1991) 3120.
11 J. D. Mackenzie, in L. L. Hench and D. R. Ulrich (eds.), *Ultrastructure Processing of Ceramics, Glasses, and Composites*, Wiley, New York, 1984, p. 15.
12 A. V. Kavuliunas, A. Taylor and R. D. Rieke, *Organometallics, 2* (1983) 377.
13 H. W. Chen, W. L. Jolly, J. Kopf and T. H. Lee *J. Am. Chem. Soc., 101* (1979) 2607.
14 D. Briggs and M. P. Seah, *Practical Surface Analysis*, John Wiley, New York, 1990, p. 607.
15 G. C. Bond, *Heterogeneous Catalysis: Principles and Applications*, Oxford University Press, New York, 1987.